Reflection FWI

Kenneth Irabor and Mike Warner, Imperial College London*

Summary

We demonstrate that FWI can successfully recover all wavelengths within a velocity model using as input only raw, multiple-contaminated, short-offset, reflection data. To do this, we isolate the tomographic and migration aspects of FWI based upon the direction of travel of the forward and residual wavefields, we alternate migration-like and tomography-like FWI iterations, and we do not retain the migration component between iterations. We follow this alternating scheme by conventional reflection FWI to recover the full-bandwidth velocity model.

Introduction

Given an adequate starting model, the recovery of missing long-wavelength components in a velocity model using full-waveform inversion is reasonably straightforward when the target area is traversed by long-offset transmitted waves (Warner et al, 2013). Recovery of shorter-wavelength components is also straightforward when the target area is illuminated by short-offset sub-critical reflected waves (Lazaratos et al., 2011). Here we explore a more-difficult problem – that of recovering both long and short-wavelength components of the velocity model using reflection data without any significant contribution from transmitted arrivals. We begin from a starting model that is not correct at the longest wavelengths, and we use raw reflection data contaminated by surface multiples.

Conventional FWI contains aspects that resemble both tomography and migration. FWI will produce long-wavelength tomography-like model updates when the forward and residual wavefields travel through the model together in the same direction, and it will produce short-wavelength migration-like updates when forward and residual wavefields travel in different directions (Tang et al, 2013). In smooth starting models, only transmitted arrivals can generate tomographic velocity updates; in such models, reflected arrivals produce only migration-like updates. In rough starting models, that already contain reflectors, reflected arrivals can produce both tomographic and migration-like velocity updates. However, for typical reflection amplitudes, the strength of the migration update will normally be much larger than that of the tomographic update.

There are two problems to solve: (1) In order to obtain a tomographic update from reflection data we must first obtain a migration update in order to introduce reflectors into the velocity model – but if the long-wavelength model is not yet correct, then these reflectors will be incorrectly positioned within the model; (2) It is difficult to take advantage of the tomographic properties of reflection FWI in the presence of a strong migration update.

Method

We solve the first problem by alternating migration-like and tomography-like FWI iterations, regenerating the reflectors after each tomography-like model update. We solve the second problem by separating both source and residual wavefields according to their direction of travel.

We separate horizontally and vertically travelling wavefields by reformulating the wave equation, and we separate up-going and down-going wavefields using 2D Fourier transforms, Figure 1. We write the wave equation:

$$\frac{1}{c^2}\frac{\partial^2}{\partial t^2}(p_x + p_z) - \left[\frac{\partial^2 p}{\partial x^2} + \frac{\partial^2 p}{\partial z^2}\right] = s$$

where $p_x + p_z = p$.

This can be solved by solving the two coupled equations:

$$\frac{1}{c^2}\frac{\partial^2 p_x}{\partial t^2} - \frac{\partial^2 p}{\partial x^2} = \frac{s}{2} \quad \text{and} \quad \frac{1}{c^2}\frac{\partial^2 p_z}{\partial t^2} - \frac{\partial^2 p}{\partial z^2} = \frac{s}{2}$$

where p_z represents the vertically travelling portion of the wavefield, and p_x represents the horizontal portion. Some numerical care is needed in solving these equations, since they can allow for the growth of spurious wave-modes that vanish when the two wavefields are summed.

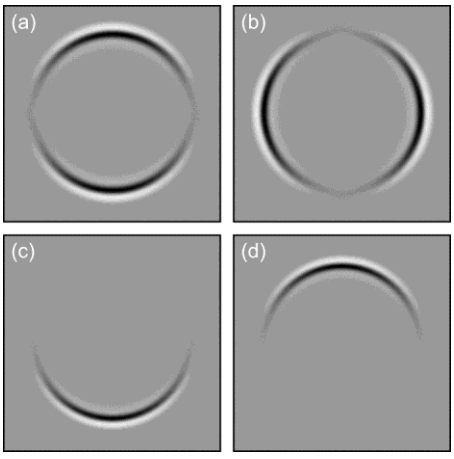

Figure 1: Wavefield separation for a single point source in a homogeneous model: (a) vertical p_z, (b) horizontal p_x, (c) down-going, and (d) up-going wavefields.

Our reflection FWI workflow then proceeds as follows:

1. Begin from low frequencies and a smooth velocity model obtained from pre-stack time migration.
2. Form a migration-like FWI update by correlating the down-going source wavefield with the up-going residual wavefield without preserving true amplitudes.
3. Using an accurate step length, form a fully quantitative tomography-like FWI update by correlating the up-going reflected source wavefield with the down-going residual wavefield. Retain this tomographic update and remove the migration update from step 2.
4. Increase the data bandwidth, and repeat from step 2.
5. Repeat all the iterations represented by steps 2 to 4, reiterating from low to high frequencies.
6. Using the model obtained from step 5, run conventional reflection-based FWI, iterating from low to high frequencies.

At step 2, we do not perform a conventional step-length calculation, instead we scale the update heuristically to obtain strong reflections. At step 5, we optionally repeat everything – the degree to which this is necessary appears to be data and model dependent.

Example

We have applied this scheme to a number of datasets; here we show the results applied to Marmousi. For this dataset, we limited the maximum offset to 3200 m. Figure 2 shows a shot record, filtered to 6.5 Hz, generated from the true model and the same record obtained from the starting model. The limited offset ensures that the data contains only the direct arrival and primary reflections, together with near-surface superficially penetrating transmitted arrivals, free-surface multiples and back-scattered refractions. It does not contain the deeper-penetrating refracted arrivals that would normally drive the long-wavelength FWI velocity update.

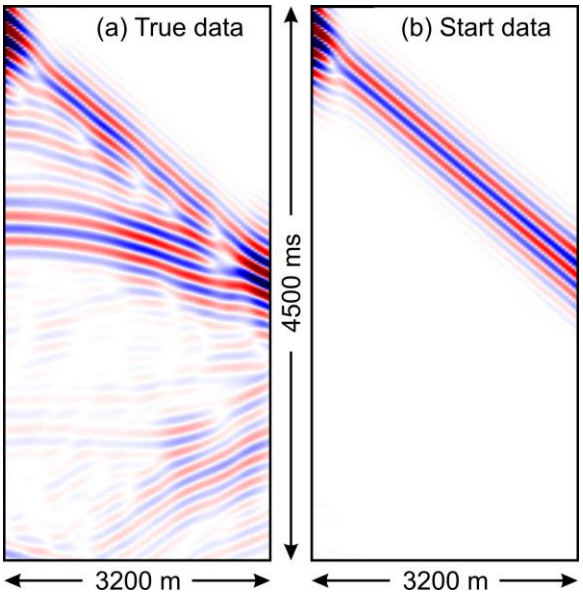

Figure 2: Limited-offset shot record used for FWI.

The true and start models are shown in Figures 3a and b. The start model contains no reflectors below the seabed, and it contributes only a single superficial transmitted arrival to the inversion. The lowest usable frequency in this dataset is at about 3.5 Hz. At this frequency, the start model is adequate for conventional FWI if long-offset, deeply penetrating transmitted arrivals are included in the input dataset, but it is not sufficiently accurate for conventional FWI if only restricted-offset reflections are included as is the case here.

We ran the inversion using two iterations of migration FWI at step 2, and five iterations of tomographic FWI at stage 3. At stage 4, we ran the inversion over ten frequency bands ranging from 3.5 to 11.5 Hz. At stage 5, we repeated the full inversion a second time, and at stage 6 we used sixty conventional iterations to produce the final velocity model.

Results

Figures 3c to f show the results of the inversion. Figure 3c shows the first migration-like FWI update applied at step 2 at 3.5 Hz. This update represents the reflectors that FWI is introducing into the model at this stage; these will be later removed from the model. The wavelengths within this update lie predominantly within the bandwidth of the input seismic data. Note that the color scales used for the updates shown in Figures 3c and d are not the same as those used to display the models themselves.

Figure 3d shows the first tomography-like FWI update applied at step 3 at 3.5 Hz. Even at this early stage, the broad regions of the model that require long-wavelength velocity adjustment can be identified. The bandwidth of this tomographic update overlaps with that of the migration update, but it also extends to longer wavelengths that lie entirely outside the bandwidth of the seismic data – this is one of the characteristics that separates tomography from migration. We note in passing, that it is not possible in this example to separate the two updates based purely on their scale lengths as proposed for example by Xu et al. (2012).

Figure 3e shows the velocity model after step 5. It contains only the cumulative effect of all the tomographic FWI iterations; the direct effects of the migration iterations have

been removed at each stage. This model does not closely resemble that which might be obtained either from conventional reflection travel-time tomography or from conventional transmission FWI. Neither does it resemble the model that would be obtained by applying conventional migration-dominated broad-band reflection FWI directly to the starting model. Instead, it contains an accurate long-wavelength representation of the true model, filtered directionally along structure, and with an additional directional bias that favors vertically aligned velocity structure. These longer wavelengths, and the vertically features, are exactly those that conventional FWI applied to reflection data is unable to capture successfully.

The final model is shown in Figure 3f. This represents conventional FWI, applied to pure reflection data, using the model from Figure 3e as the starting model. Note that the input data contains multiples and does not contain significant refracted arrivals. The result provides a good match to the true model in all portions that are adequately covered by the observed data.

Unsurprisingly, reflection FWI does not recover the velocity model accurately at the extreme left and right edges of the model where there is insufficient offset available in the observed data. It is also unable to recover the true velocity close to the base of the model. This characteristic may at first appear surprising to those more used to seeing Marmousi inverted using refracted arrivals. In that case, refracted arrivals penetrate to the base of the model, and the model there can be recovered fully. However, when using pure reflections, as we have done here, no arrivals penetrate below the deepest reflector, and so the observed reflection data contain no information about the model close to its base.

Figure 4 shows a synthetic shot record generated by the true model and by the final FWI-recovered model. The figure shows both the short-offset data that were used to drive the inversion, and longer-offset data that can be predicted from both models but that were not used at any stage in the inversion. The short-offset match between the two datasets is good. More surprisingly perhaps, the long-offset data also match well, though in fine detail the match is less good than we would expect to have obtained if these data had also been included directly in the inversion.

Discussion and Conclusions

We have demonstrated a scheme that is able to invert pure reflection data successfully, using FWI, in circumstances and with a starting model for which conventional reflection FWI is unable to recover the long-wavelength velocity model. The scheme does not require multiple-free data, and we have here inverted data with all

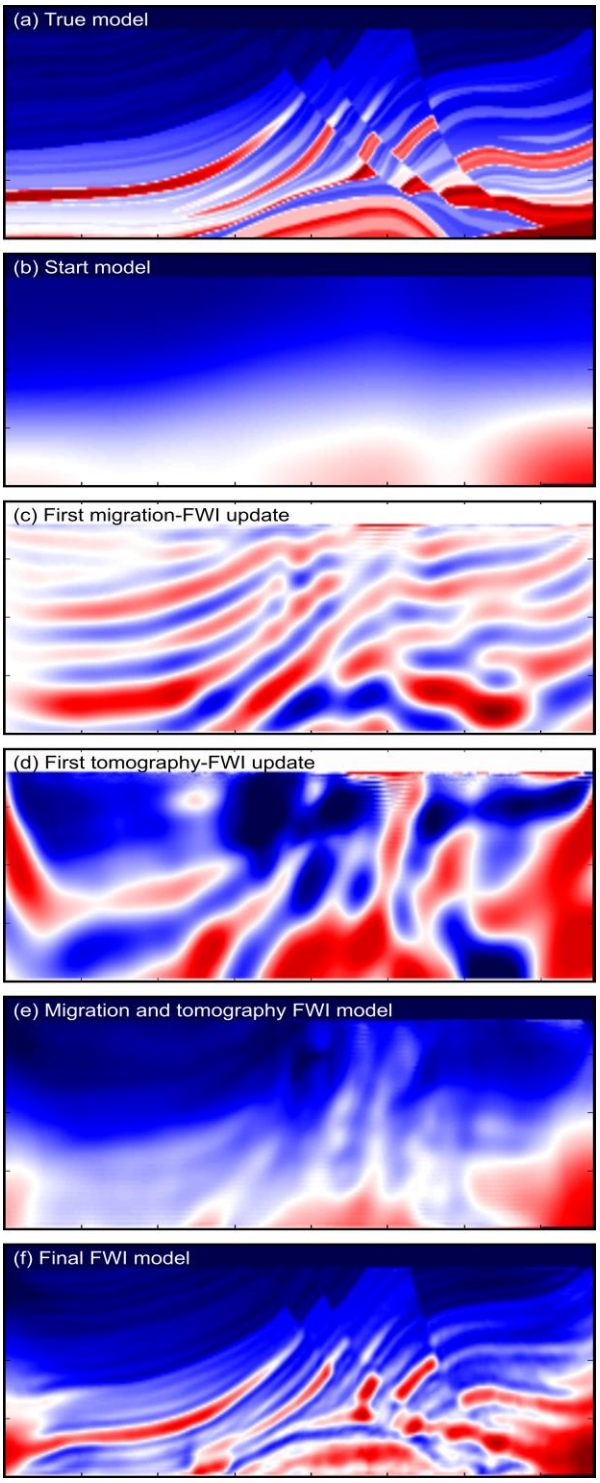

Figure 3: Reflection FWI results – see text for details.

free-surface and interbed multiples present. The scheme does not require ghosts, direct and shallow refracted arrivals to be removed, nor does it require a zero-phase wavelet. The scheme is effective when the maximum source-receiver offset available is about one-and-a-half that of the target depth.

The scheme begins from a reasonably accurate starting model that is adequate for pre-stack time migration, but it does not require a model that is extremely accurate at long-wavelengths. Unlike conventional FWI when applied to pure reflection data, the scheme is able to recover the velocity model at wavelengths that lie significantly outside that of the input seismic reflection data.

Significantly, this inversion scheme does not require or seek to match the absolute amplitudes of reflections in order to be effective. Indeed, the migration step in our inversion is not true amplitude, and this does not negatively impact the inversion. If we seek to make the migration true amplitude by incorporating a fully quantitative conventional step-length calculation to scale the update, then this significantly increases the number of iterations required at the least-squares migration FWI step (our step 2) with no consequent improvement in the quality of the final model.

The absence of a requirement to match amplitudes accurately is important since this is difficult to achieve in practice without significant additional information and control – for example from wells. This is because density, attenuation, shear-wave velocity, sub-wavelength layering, and short-wavelength anisotropy variations, can all affect reflection amplitudes in ways that do not directly impact the velocity model. Since our scheme does not seek to match amplitudes accurately, it is not so readily subject to the uncertainties that these additional unknown parameters can introduce.

We have demonstrated the scheme here without any consideration of anisotropy. It is however straightforward to include inversion for anisotropic parameters into our approach, either through a local gradient-based inversion (da Silva et al., 2014), or through an initial global inversion for anisotropy (Debens et al., 2015).

The computational cost of our reflection FWI scheme is about three times that of a conventional transmission FWI scheme on the same dataset. However, in practice, the application of transmission FWI to the target depths that reflection FWI can reach, requires source-receiver offsets to be about three times or more than those needed for reflection FWI. In these circumstances then, the compute cost of the two methods becomes similar, and, more significantly, the acquisition cost for the reflection version is much reduced.

Acknowledgements

This work forms part of the Fullwave Game Changer research program at Imperial College. We thank the sponsors of that JIP for their continuing support.

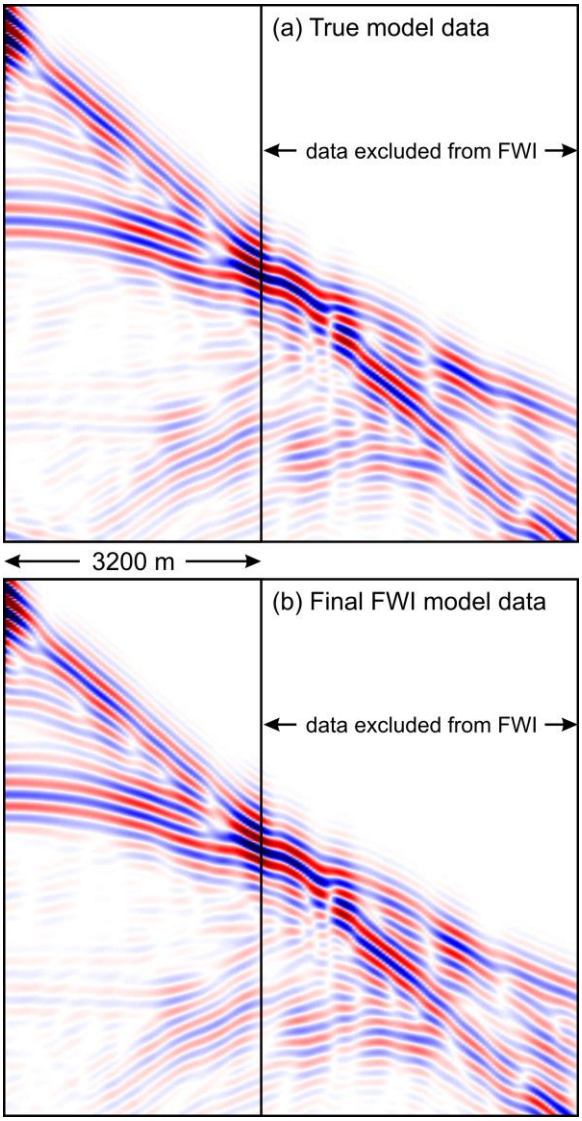

Figure 4: Extended-offset shot record from (a) the true model, and (b) the final FWI model. Only data with an offset less than 3200 m was included in the inversion. Nonetheless the resultant reflection FWI model is still able to predict the observed longer-offset data accurately.

EDITED REFERENCES

Note: This reference list is a copyedited version of the reference list submitted by the author. Reference lists for the 2016 SEG Technical Program Expanded Abstracts have been copyedited so that references provided with the online metadata for each paper will achieve a high degree of linking to cited sources that appear on the Web.

REFERENCES

Debens, H. A., M. Warner, A. Umpleby, and N. V. da Silva, 2015, Global anisotropic 3D FWI: 85th Annual International Meeting, SEG, Expanded Abstracts, 1193–1197, http://dx.doi.org/10.1190/segam2015-5921944.1.

da Silva, N. V., A. Ratcliffe, G. Conroy, V. Vinje, and G. Body, 2014, A new parameterization for anisotropy update in full waveform inversion: 84th Annual International Meeting, SEG, Expanded Abstracts, 1050–1055, http://dx.doi.org/10.1190/segam2014-0664.1.

Lazaratos, S., I. Chikichev, and K. Wang, 2011, Improving the convergence rate of full wavefield inversion using spectral shaping: 81st Annual International Meeting, SEG, Expanded Abstracts, 2428–2432, http://dx.doi.org/10.1190/1.3627696.

Tang, Y., S. Lee, A. Baumstein, and D. Hinkley, 2013, Tomographically enhanced full wavefield inversion: 83rd Annual International Meeting, SEG, Expanded Abstracts, 1037–1041, http://dx.doi.org/10.1190/segam2013-1145.1.

Warner, M., A. Ratcliffe, T. Nangoo, J. Morgan, A. Umpleby, N. Shah, V. Vinje, I. Štekl, L. Guasch, C. Win, G. Conroy, and A. Bertrand, 2013, Anisotropic 3D full-waveform inversion: Geophysics, **78**, no. 2, R59–R80, http://dx.doi.org/10.1190/geo2012-0338.1.